ELSEVIER

Journal of Magnetism and Magnetic Materials 192 (1999) 325–333

Journal of magnetism and magnetic materials

FLAPW calculations of the magneto-optical Kerr effect of BCC Fe

Hiromu Miyazawa, Tamio Oguchi*

Department of Quantum Matter, ADSM, Hiroshima University, 1-3-1 Kagamiyama, Higashi-Hiroshima 739-8526, Japan

Received 25 August 1998; received in revised form 15 October 1998

Abstract

Magneto-optical Kerr effect (MOKE) of BCC Fe is calculated beyond the visible-light energy up to 27 eV by means of the full-potential linear augmented plane wave (FLAPW) method within the local spin-density approximation. Calculated MOKE spectra are in good agreement especially for the high-energy region with recently reported experimental results, which have shown a qualitative discrepancy with previous augmented-spherical-wave results. A new peak in the MOKE spectra is found around 18 eV. Convergence properties of several parameters included in our FLAPW scheme are also studied.

Keywords: Magneto-optical Kerr effect; First-principles calculation; BCC Fe; FLAPW method

1. Introduction

Local spin-density-approximation (LSDA) calculations of the magneto-optical Kerr effect (MOKE) have been extensively carried out in last decade for various kinds of ferromagnetic materials such as transition metals [1–3], transition-metal compounds [4–10] and multilayers [11–14], and rare-earth and actinide compounds [15–17]. All of the calculations are based on the Kubo formula of the optical conductivity proposed by Wang and Callaway [18,19]. It is now well recognized that the LSDA calculation provides not only a very powerful tool to investigate the microscopic origins of MOKE from first principles but also a rigorous evaluation of the one-electron approximation and numerical techniques involved in direct comparison with experiment.

In the MOKE calculations so far reported, linear muffin-tin orbital (LMTO) and augmented spherical wave (ASW) methods were used to obtain one-electron eigenvalues and eigenfunctions. The LMTO and ASW methods are known to be very efficient because of using a minimal basis set, compared with plane-wave base methods. The calculated MOKE results indeed indicate that the LMTO and ASW methods are highly efficient and accurate to calculate MOKE for a wide range of ferromagnetic materials within the visible-light energy range.

Very recently, MOKE spectra have been measured for BCC Fe in a photon energy up to 10 eV

* Corresponding author. Tel.: + 81-824-24-7393; fax: + 81-824-24-7395; e-mail: oguchi@ipc.hiroshima-u.ac.jp.

0304-8853/99/$ – see front matter
PII: S0304-8853(98)00535-6

by using a synchrotron radiation source [20] and shown a qualitatively different result from the previous ASW calculations. It is not clear whether the discrepancy arises from LSDA or other numerical methods such as ASW. To answer this is one of our aims in the present paper. We have formulated the optical conductivity by means of the full-potential linear augmented plane wave (FLAPW) method and calculated MOKE for BCC Fe in the photon energy up to 27 eV. The calculated spectra are in good agreement with the recent MOKE data, indicating the importance of representation for nearly free-electron-like unoccupied states in evaluating MOKE in a higher energy than the visible light. Furthermore, it has also been observed that the MOKE spectra show an orientation dependence in the (0 0 1)- and (1 1 0)-plane-grown films [20]. We have studied the dependence by changing the magnetization axis from the [0 0 1] to [1 1 0] direction.

2. Methods

Within LSDA, one-electron Kohn–Sham equations are solved self-consistently by using the FLAPW method [21–23]. We employ particularly the basis-set construction and iterative algorithm proposed by Soler and Williams [24–26].

A spin–orbit coupling (SOC), $\mathscr{H}_{\mathrm{so}}$, which is neglected in scalar-relativistic LSDA calculations [27], is essential to obtain the orbital magnetic moment and consequently the magneto-optical effects. The SOC term may be incorporated as a second variation in the LSDA calculation. The relativistic wave functions $\Psi_n(\boldsymbol{k}, \boldsymbol{r})$ can be expanded with unperturbed wave functions $\psi_i^{\sigma}(\boldsymbol{k}, \boldsymbol{r})$ as

$$\Psi_n(\boldsymbol{k}, \boldsymbol{r}) = \sum_{i,\sigma} \psi_i^{\sigma}(\boldsymbol{k}, \boldsymbol{r}) C_{i\sigma,n}(\boldsymbol{k}). \tag{1}$$

The expansion coefficients $C_{i\sigma,n}(\boldsymbol{k})$ are determined by solving one-electron equations:

$$[\mathscr{H}_0 + \mathscr{H}_{\mathrm{so}}]\Psi_n(\boldsymbol{k}, \boldsymbol{r}) = \varepsilon_n(\boldsymbol{k})\Psi_n(\boldsymbol{k}, \boldsymbol{r}), \tag{2}$$

with the corresponding relativistic eigenvalues $\varepsilon_n(\boldsymbol{k})$.

The existence of the magnetic moment with SOC results in certain difference in the phase shift of reflectance or absorption between left and right-circularly polarized lights which are called magneto-optical effects. In particular, MOKE is the magneto-optical effect appearing in the reflectance spectra and used widely as a reading method in magneto-optical devices. In order to evaluate MOKE from first principles, the transition probability of electrons excited by a photon should be calculated. The optical conductivity tensor due to the interband transition can be obtained by applying the Kubo formula of the linear response theory [18] as

$$\sigma_{\alpha\beta}(\omega) = -\frac{2ie^2}{m^2\hbar}\sum_{\boldsymbol{k}}\sum_{n,n'}\left(\frac{\omega + \mathrm{i}/\tau}{\omega_{n'n}(\boldsymbol{k})}\,\mathrm{Re}[\pi^{\alpha}_{nn'}(\boldsymbol{k})\pi^{\beta}_{n'n}(\boldsymbol{k})] + \mathrm{i}\,\mathrm{Im}[\pi^{\alpha}_{nn'}(\boldsymbol{k})\pi^{\beta}_{n'n}(\boldsymbol{k}Z)]\right)\frac{1}{\omega^2_{n'n}(\boldsymbol{k}) - (\omega + \mathrm{i}/\tau)^2}, \tag{3}$$

where τ is the relaxation time of the excited electron. Assuming an appropriate value for τ, the real and imarginary parts of $\sigma_{\alpha\beta}(\omega)$ are derived directly from Eq. (3). $\pi^{\alpha}_{nn'}(\boldsymbol{k})$ is the matrix element of the α component of a momentum operator $\hat{p} = -\mathrm{i}\hbar\nabla$:

$$\pi^{\alpha}_{nn'}(\boldsymbol{k}) = \int \mathrm{d}\boldsymbol{r}\ \Psi^{*}_{n}(\boldsymbol{k}, \boldsymbol{r})\hat{p}_{\alpha}\Psi_{n'}(\boldsymbol{k}, \boldsymbol{r}) \tag{4}$$

and $\omega_{nn'}$ is the energy difference between occupied (n) and unoccupied (n') states

$$\hbar\omega_{n'n}(\boldsymbol{k}) = \varepsilon_{n'}(\boldsymbol{k}) - \varepsilon_n(\boldsymbol{k}). \tag{5}$$

According to our choice of the FLAPW basis set, the wave functions of Eq. (1) can be expressed as

$$\Psi_j(\boldsymbol{k}, \boldsymbol{r}) = \tilde{\Psi}_j(\boldsymbol{k}, \boldsymbol{r}) + \sum_{v}\sum_{\ell m}^{\ell_{\max}}[\Psi_{v\ell mj}(\boldsymbol{k}, \boldsymbol{r}_v) - \tilde{\Psi}_{v\ell mj}(\boldsymbol{k}, \boldsymbol{r}_v)], \tag{6}$$

where $\tilde{\Psi}_j(\boldsymbol{k}, \boldsymbol{r})$ and $\tilde{\Psi}_{v\ell mj}(\boldsymbol{k}, \boldsymbol{r}_v)$ are the plane-wave (Fourier) part defined in the whole space and its spherical-wave (ℓm) expansion inside a sphere around atom v, respectively, and $\Psi_{v\ell mj}(\boldsymbol{k}, \boldsymbol{r}_v)$ is the spherical-wave part defined inside the sphere with the cutoff of $\ell_{\max}$. In Eq. (6), $\sum_{\ell m}^{\ell_{\max}}$ stands for $\sum_{\ell=0}^{\ell_{\max}}\sum_{m=-\ell}^{m=\ell}$. With use of the wave functions in Eq. (6), the matrix element in Eq. (4) may be given by

the following three terms:

$$\pi_{nn'}(\boldsymbol{k}) = \pi^{(1)}_{nn'} + \pi^{(2)}_{nn'} + \pi^{(3)}_{nn'}, \tag{7}$$

$$\pi^{(1)}_{nn'} = \int \mathrm{d}\boldsymbol{r}\ \tilde{\Psi}^*_n \hat{p} \tilde{\Psi}_{n'}, \tag{8}$$

$$\pi^{(2)}_{nn'} = \int \mathrm{d}\boldsymbol{r} \sum_{\nu} \sum_{\ell m}^{\ell_{\max}} \sum_{\ell' m'}^{\ell_{\max}} [\Psi^*_{\nu\ell mn} \hat{p} \Psi_{\nu\ell' m' n'} - \tilde{\Psi}^*_{\nu\ell mn} \hat{p} \tilde{\Psi}_{\nu\ell' m' n'}], \tag{9}$$

$$\pi^{(3)}_{nn'} = \int \mathrm{d}\boldsymbol{r} \sum_{\nu} \sum_{\ell m}^{\ell_{\max}} \sum_{\ell' m' (>\ell_{\max})}^{\infty} (\tilde{\Psi}_{\nu\ell' m' n} \hat{p} [\Psi_{\nu\ell mn'} - \tilde{\Psi}_{\nu\ell mn'}] + [\Psi_{\nu\ell mn} - \tilde{\Psi}_{\nu\ell mn}]^* \hat{p} \tilde{\Psi}_{\nu\ell' m' n'}). \tag{10}$$

Since the dipole transition may be allowed only between the spherical waves with $|\ell - \ell'| = 1$, the matrix elements for $\ell = \ell_{\max}$ and $\ell' = \ell_{\max} + 1$ remain in Eq. (10). Furthermore, it is expected that the $\pi^{(3)}_{nn'}$ term may be much smaller than the other two terms because $\Psi_{\nu\ell mn} - \tilde{\Psi}_{\nu\ell mn}$ has a very small magnitude due to the continuity conditions near the sphere boundary where $\tilde{\Psi}_{\nu\ell mn}$ has a maximum. Therefore, we neglect the $\pi^{(3)}_{nn'}$ term in the present calculation. To check this, the convergence with respect to $\ell_{\max}$ will be examined in detail in the following section. The matrix element of a momentum operator becomes Hermitian because $\pi^{(1)}_{nn'}$ is Hermitian obviously and $\pi^{(2)}_{nn'}$ is Hermitian by virtue of the continuation condition between $\Psi_{\nu\ell mn}$ and $\tilde{\Psi}_{\nu\ell mn}$ at the muffin-tin sphere surface.

Finally, the Kerr rotation angle $\theta_{\mathrm{K}}(\omega)$ and its ellipticity $\eta_{\mathrm{K}}(\omega)$ are defined as

$$\theta_{\mathrm{K}}(\omega) + \mathrm{i}\eta_{\mathrm{K}}(\omega) = -\frac{\sigma_{xy}(\omega)}{\sigma_{xx}(\omega)\sqrt{1 + \mathrm{i}(4\pi/\omega)\sigma_{xx}(\omega)}} \tag{11}$$

in the case of the magnetization axis and the incident light parallel to the z direction.

Besides the interband term described above, the intraband contribution to the conductivity must be included in metallic cases and may be additionally treated within a phenomenological expression by Drude. However, since an empirical plasma energy introduces another ambiguity into the shape of the spectrum especially in low-energy regions and its effects on the spectrum have been already investigated in the case of BCC Fe [1], the intraband contribution will not be considered in the present study.

In order to compute the optical conductivity accurately, the $\boldsymbol{k}$ integration must be greatly taken care of. We adopt the improved tetrahedron method [28] and investigate the accuracy by changing the number of $\boldsymbol{k}$ points $N_{\boldsymbol{k}}$ up to $18 \times 18 \times 18 = 5832$ in the full Brillouin zone. One can get the spin magnetic moment within 0.01 μ_{B} and the Kerr rotation angle and ellipticity up to 1 Ry within a few hundredth degrees with $N_{\boldsymbol{k}} = 14 \times 14 \times 14 = 2744$.

Next we have checked the convergence about the number of states included in the second variation in Eq. (1). It is found that 10 states per spin are enough to describe the spectra up to 1.0 Ry while 15 states are needed for high-energy spectra up to 2 Ry. This fast convergence may be because of the weakness of the perturbation $\mathscr{H}_{\mathrm{so}}$ in comparison to the energy difference between the electron states in the higher-energy region where electrons behave like nearly free electron.

3. A test of the spherical-wave expansion

In this section, we examine the convergence in the optical conductivity and the Kerr spectra with respect to the maximum angular momentum in the spherical-wave expansion $\ell_{\max}$ in Eq. (6). In the present test for BCC Fe, we commonly use the lattice constant of $a = 2.87$ Å, the muffin-tin radius of 1.1 Å, the relaxation-rate parameter $\hbar\delta \equiv \hbar/\tau = 0.04$ Ry, the cutoff energy of 15 Ry for the basis functions (the corresponding cutoff of 60 Ry for the charge density and potential functions) and $N_{\boldsymbol{k}} = 18 \times 18 \times 18 = 5832$.

Figs. 1 and 2 show the optical conductivity and Kerr spectra calculated for BCC Fe by changing $\ell_{\max}$ from 2–4. It is seen in Figs. 1 and 2 that the difference between $\ell_{\max} = 3$ and 4 is negligibly small and that $\ell_{\max} = 2$ may be almost sufficient for qualitative discussions of the Kerr spectra though the optical conductivity shows somewhat large (at most 20%) difference between $\ell_{\max} = 2$ and 3. The negligible difference between $\ell_{\max} = 3$ and 4 indicates that the $\ell \geqslant 3$ states are well expressed by the plane waves and the $\pi^{(3)}_{nn'}$ term in the matrix

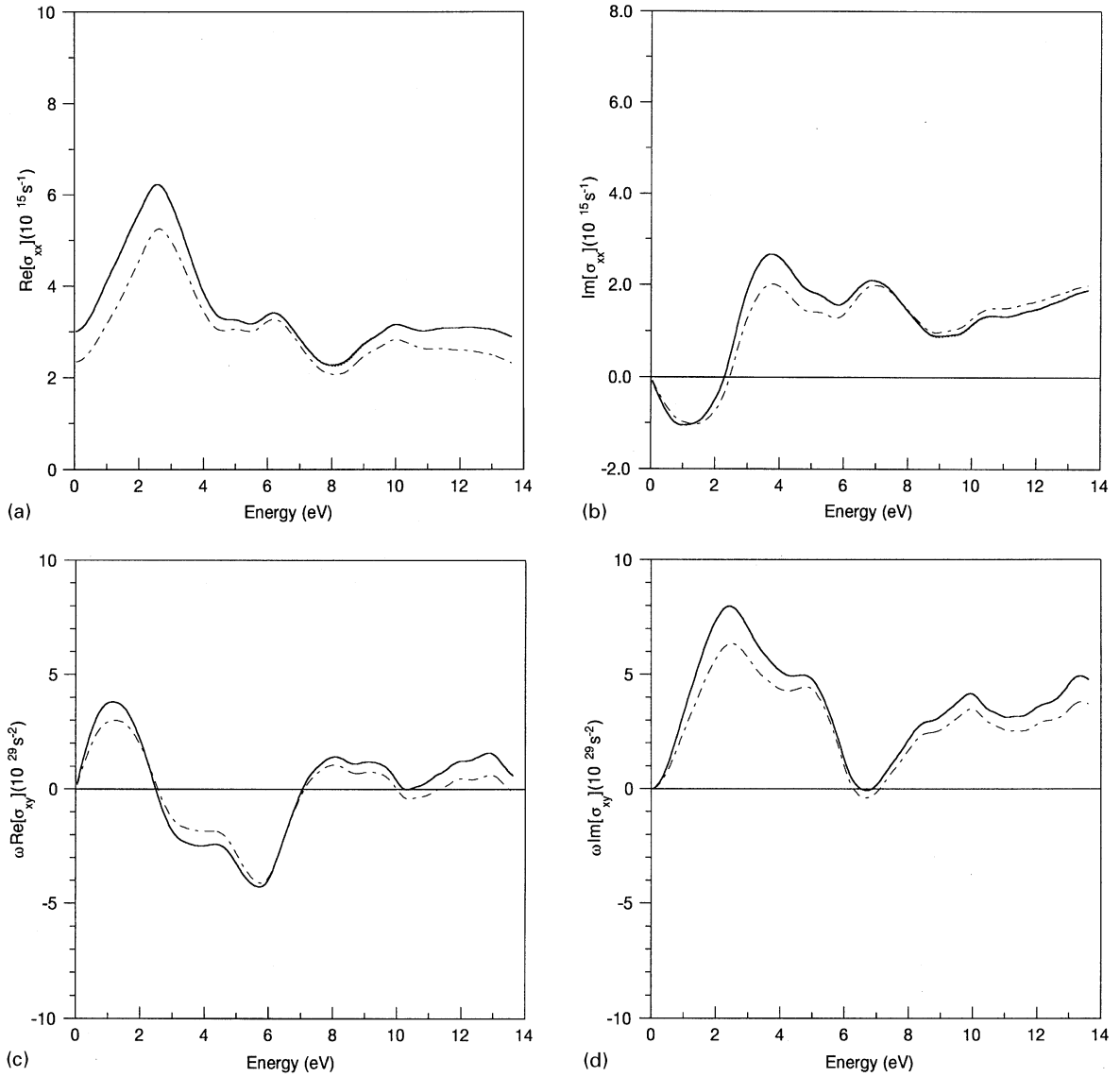

Fig. 1. Calculated optical conductivity of BCC Fe: (a) the real part of σ_{xx}, (b) the imaginary part of σ_{xx}, (c) the real part of $\omega\sigma_{xy}$ and (d) the imaginary part of $\omega\sigma_{xy}$ with $\ell_{\max} = 2$ (dash–dotted line), $\ell_{\max} = 3$ (solid line) and $\ell_{\max} = 4$ (dotted line). An intraband contribution is not included.

elements can be neglected. The difference between $\ell_{\max} = 2$ and 3 is mostly due to an error caused by the neglect of $\pi^{(3)}_{nn'}$, assuming the $\ell = 3$ states are well represented by the plane waves. In the case of $\ell_{\max} = 2$, important d–f or f–d transitions should be given by the $\pi^{(3)}_{nn'}$ term, because the plane-wave representation of the $\ell = 2$ states are definitely insufficient.

Concerning the description of the electronic states, the conventional FLAPW method requires a high $\ell_{\max}$ value to connect the wave functions smoothly at the muffin-tin sphere. For example,

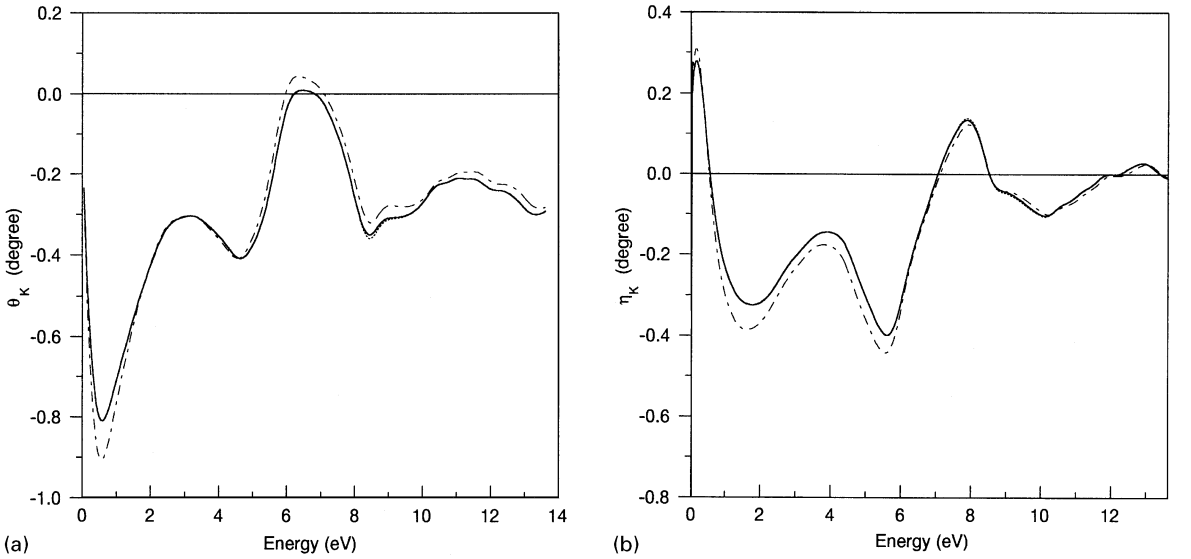

Fig. 2. Calculated spectra of (a) Kerr rotation angle and (b) Kerr ellipticity of BCC Fe with $\ell_{max} = 2$ (dash–dotted line), $\ell_{max} = 3$ (solid line) and $\ell_{max} = 4$ (dotted line). An intraband contribution is not included.

Hathaway et al. [29] adopted $\ell_{max} = 8$ for BCC Fe. This is because that discontinuity in the wave functions and the charge density may lead to an inaccurate solution in the self-consistent procedure. In our formulation, $\ell_{max} = 2$ is enough to get the accurate electronic states since states with ℓ larger than ℓ_{max} are expressed by the plane waves.

This feature of our FLAPW basis functions provides another advantage to represent wave functions properly in high-energy regions where the linear method may break down within a single-energy window [21,22]. Electronic states in the high-energy region are basically nearly free-electron like. The states with $\ell > \ell_{max}$ inside the muffin-tin sphere are not restricted by the linear method in our formulation since they can be expressed by the plane-wave functions penetrating into the sphere. The states with $\ell \leqslant \ell_{max}$ are expected to have very small amplitudes within the muffin-tin sphere in the high-energy region. The present linear method is suitable to express the electronic states precisely and efficiently in the high-energy region.

The spherical-wave expansion must depend on the sphere radius assumed and the results shown above may change by choosing another radius. Fig. 3 shows the Kerr spectra calculated with the sphere radius of 1.24 Å, which corresponds to the inscribed sphere radius of the present BCC lattice. No definite difference can be seen in Fig. 3 except for minor ones around 10 eV. It is, therefore, concluded that the present FLAPW scheme for calculating the Kerr spectra is robust in the sense that the calculated results are independent of the parameters involved within their physically reasonable and computationally efficient range.

4. Results and discussions

Theoretical and experimental Kerr spectra are shown in Fig. 4 for comparison. It can be found that general features of the observed spectra are well reproduced by the present FLAPW calculation. In the Kerr spectrum, peaks at 4.5 and 6.0 eV coincide with Katayama's data. A shoulder near 7.4 eV is slightly shifted to a higher energy region by 0.7 eV in this work. As shown in Fig. 4, the ASW spectrum reveals a deviation above 6 eV. It is seen that qualitative agreement of the

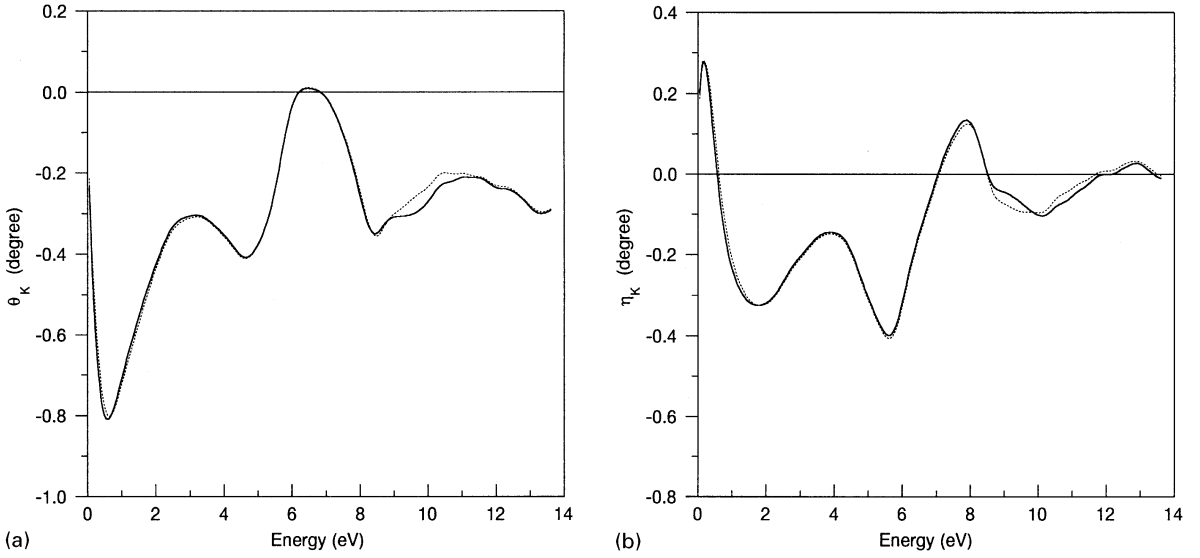

Fig. 3. Calculated spectra of (a) Kerr rotation angle and (b) Kerr ellipticity of BCC Fe with the muffin-tin radii of 1.24 Å (dotted line) and 1.1 Å (solid line). An intraband contribution is not included.

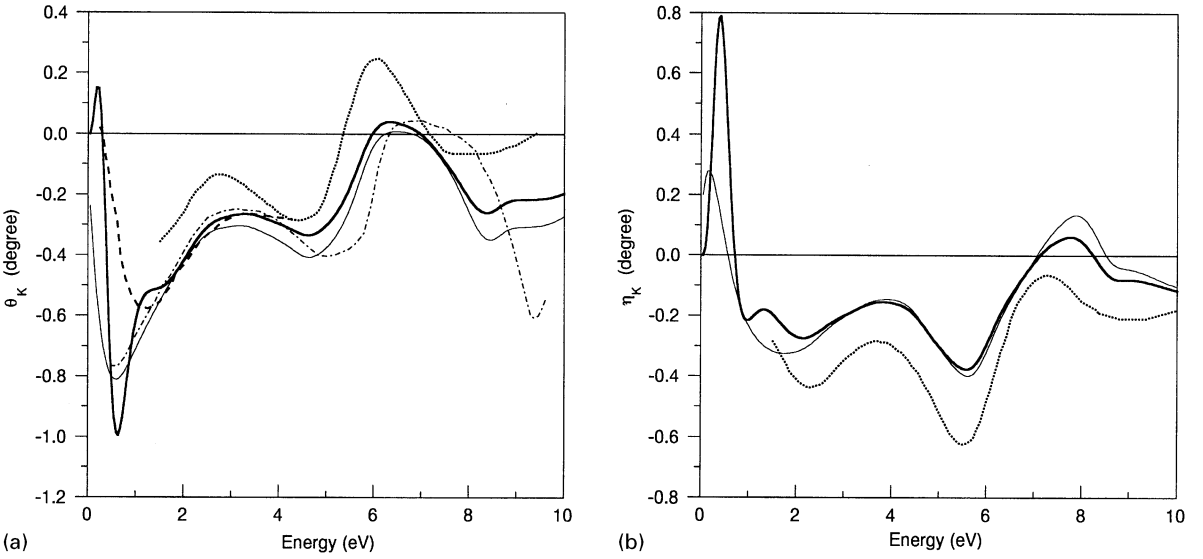

Fig. 4. Calculated (thin solid line) spectra of (a) Kerr rotation angle and (b) Kerr ellipticity of BCC Fe with experimental results by Katayama (dotted line) [20] and by Krinchik (dashed line) [38]. Thick solid lines denote calculated Kerr spectra with the correction by the virtual refractive-index method along the experimental film structure (Au capping layer [20 Å]/Fe film [1000 Å]/Au substrate). A previous ASW result [1] is also plotted by a dash–dotted line. In the theoretical spectra, an intraband contribution in Fe is not included while that in Au is considered.

present FLAPW results with the experimental spectra above 6 eV is much better than in the case of the ASW result, in which the position of the shoulder is shifted by 1.7 eV. However, compared with Katayama's data, the absolute values of our calculated spectra are almost rigidly shifted by about 200 m degrees to a positive side in the Kerr ellipticity and to a negative side in the Kerr rotation angle. We examined effects of the capping layer and the substrate of Au used in the experiment by the virtual refractive-index method and found certain improvement by at most 100 m degrees towards the experimental spectra, as shown in Fig. 4.

Calculated MOKE spectra in a wide energy range up to 27 eV are shown in Fig. 5. Since the shallowest 3p core states are situated far below it, transitions from the core states do not affect the MOKE spectra in this survey. In Fig. 5, the Kerr spectrum of Fe can be classified into two regions based on the character of its final states by inspecting the matrix elements [30]. The low-energy region of the spectrum less than about 7 eV is characterized by the final states with d symmetry, and by those with s, p and f symmetry as tails of the neighboring d states. On the other hand, the high-energy region above 7 eV has those characterized only by the free-electron-like states.

Fig. 5 indicates three remarkable peaks in the high-energy region, which have never been discussed so far. The largest peak is situated around 18 eV. This peak can be assigned to the optical transition around H and N points in the Brillouin zone, where flat energy bands exist near 17–18 eV above the Fermi energy [30]. Two other small peaks are located around 8 and 25 eV. The peak around 8 eV has been observed in Katayama's experiment as shown in Fig. 4. This peak may be attributed to the transitions around N points because there exist flat bands near 7–8 eV above the Fermi energy at N points. The peak around 25 eV also corresponds to the transitions around N points because of flat bands near 24–25 eV above the Fermi energy at N points.

Like these features, there must exist fruitful structures in the ultra-violet region in the other materials and such surveys are now undertaken. This complex structure of the MOKE spectrum, or the off-diagonal part of the optical conductivity in the wide-energy range provides us opportunity to study the excited states in metallic systems. In addition, we can evaluate the approximation involved in the first-principles calculation by comparing with experiment directly. Thus it is strongly desired to measure the MOKE spectrum in a wide-energy range.

Katayama reported the orientation dependence of the MOKE spectra between the [0 0 1] and [1 1 0] directions [20]. However, almost no orientation dependence has been found. This should be due to weak $\mathscr{H}_{so}$ and the isotropic nature of the crystal field of BCC Fe. This kind of poor orientation dependence has been already reported for FCC Co theoretically [3] and experimentally [31]. Symmetry breaking by a lattice distortion may be important for describing the variation observed in film-grown samples.

The main difficulty to calculate the MOKE for metallic systems comes from the existence of the free-electron-like response accompanied by the Fermi surface. Generally this response, the intraband transition, is approximated by the Drude term with one parameter, the plasma energy or the optical mass. However, the optical mass should be $\boldsymbol{k}$ dependent in nature as derived by Wang and Callaway [18]. In addition to this, the Drude term affects MOKE spectra non-linearly in the low-energy region with large amount, for example under 3 eV in BCC Fe. Thus unless we obtain accurate values for the diagonal elements of the optical conductivity, the Drude term may trick us even in the case of qualitative estimation of the spectra. As well known, the LSDA limits accurate descriptions of the excited states. One example is the reflectance spectra of Cu, Ag and Au. Theory underestimates the plasma resonance energy lower by 0.3–0.8 eV as compared with experiment [32]. This error comes from the fact that LSDA estimates the d-band position shallower than the experimental one [33]. Another example can be seen in the overestimation of the d-band width of transition metals [34]. To overcome these problems arising from LSDA, one has to evaluate the self-energy, for instance, by using the GW method [35–37].

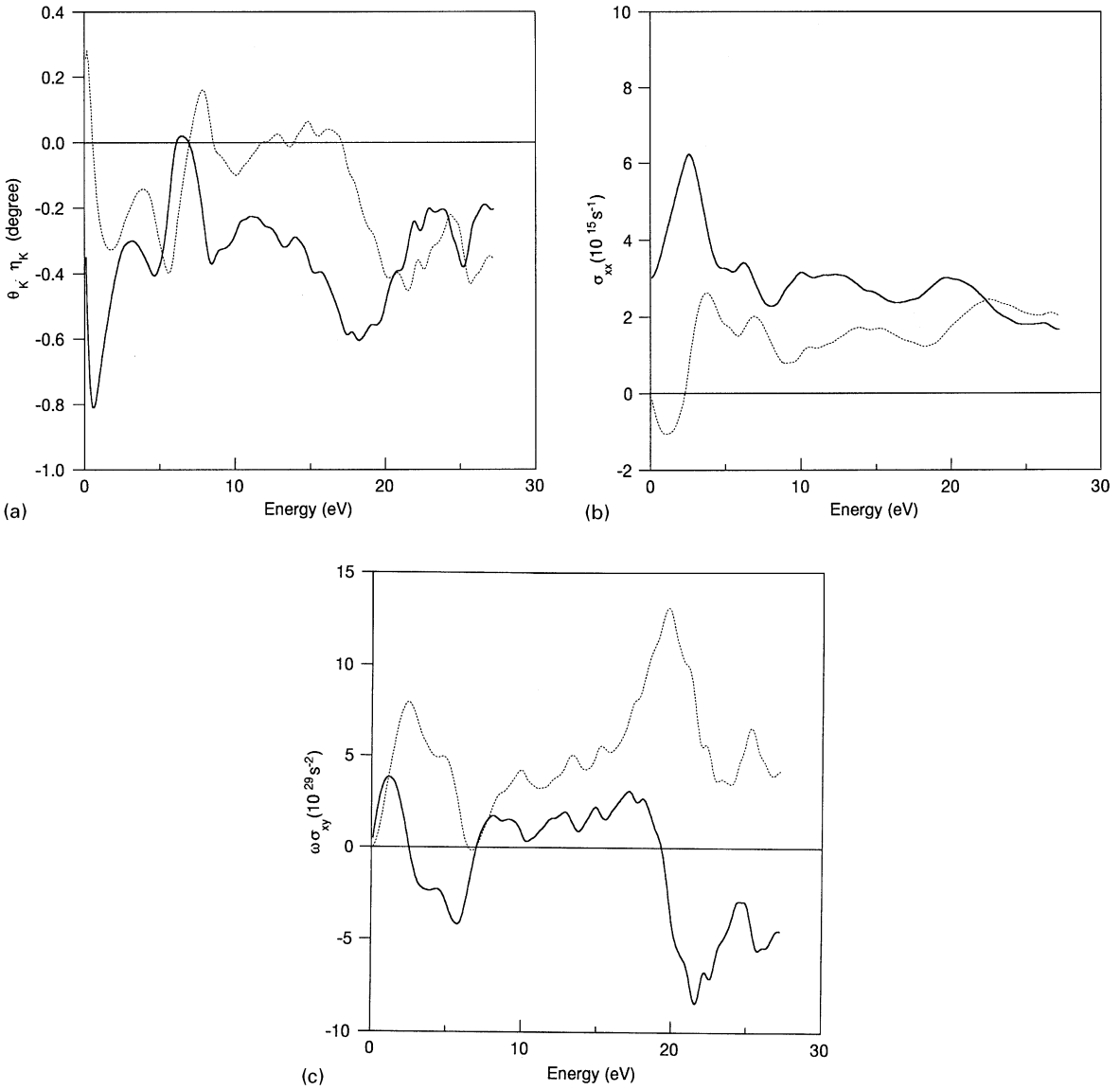

Fig. 5. Calculated Kerr spectra and optical conductivity spectra of BCC Fe up to 27 eV: (a) Kerr rotation angle (solid line) and Kerr ellipticity (dotted line), (b) the real part of σ_{xx} (solid line) and the imaginary part of σ_{xx} (dotted line), and (c) the real part of $\omega\sigma_{xy}$ (solid line) and the imaginary part of $\omega\sigma_{xy}$ (dotted line). An intraband contribution is not included.

5. Summary

We have developed a precise and efficient scheme for calculating MOKE by adopting FLAPW method within LSDA. We have checked our method by applying it to BCC Fe. Firstly, the convergence properties with respect to both $\boldsymbol{k}$ points and second-variation states are well confirmed. Secondly, as for the convergence for the spherical-wave expansion, $\ell_{\max} = 2$ is enough to obtain the accurate electronic states in our formulation. We need, however, $\ell_{\max} = 3$ when neglecting

$\pi^{(3)}_{nn'}$ in the matrix elements since the optical transitions for BCC Fe include the significant contribution of d–f transitions. It has also been found that the muffin-tin radius dependence is negligible.

We have well reproduced the MOKE spectra in the visible-light region. Another MOKE peak around 18 eV is found by our wide-energy survey. The reported orientation dependence of the MOKE spectra between [0 0 1] and [1 1 0] has not been found in our calculation.

The FLAPW method is one of the most precise techniques to calculate the electronic states especially for low-symmetry systems. Thus the MOKE calculation by adopting the FLAPW method will be a powerful tool for surface, thin layer and less-dense material systems. Applications of the present scheme to metallic multilayers such as Co/Pt, Fe/Au and Fe/Pt are now underway. Since there are many possibilities of new MOKE peaks at a high-energy region as we found in BCC Fe, a combination of high-energy experiments with synchrotron radiation lights and precise first-principles methods enables us to gain profound knowledge about microscopic relations between the electronic structure and MOKE.

Acknowledgements

The authors would like to thank T. Katayama for invaluable discussions. This work was supported by Grand-in-Aid for Scientific Research in Priority Area 'Nanoscale Magnetism and Transport' No. 281, Ministry of Education, Science, Sports and Culture. The numerical computations were performed on the Supercomputing Centers at the Institute for Solid State Physics, The University of Tokyo, and at Japan Science and Technology Corporation.

References

[1] P.M. Oppeneer, T. Maurer, J. Sticht, J. Kübler, Phys. Rev. B 45 (1992) 10924.
[2] P.M. Oppeneer, T. Kraft, H. Eschrig, J. Magn. Magn. Mater. 148 (1995) 298.
[3] P.M. Oppeneer, T. Kraft, H. Eschrig, Phys. Rev. B 52 (1995) 3577.
[4] H. Ebert, H. Akai, J. Appl. Phys. 67 (1990) 4798.
[5] I. Osterloh, P.M. Oppeneer, J. Sticht, J. Kübler, J. Phys.: Condens. Matter 6 (1994) 285.
[6] J. Kübler, J. Phys. Chem. Solids 56 (1995) 1529.
[7] P.M. Oppeneer, V.N. Antonov, T. Kraft, H. Eschrig, A.N. Yaresko, A.Ya. Perlov, Solid State Commun. 94 (1995) 255.
[8] P.M. Oppeneer, V.N. Antonov, T. Kraft, H. Eschrig, A.N. Yaresko, A.Ya. Perlov, J. Appl. Phys. 80 (1996) 1099.
[9] P.M. Oppeneer, V.N. Antonov, T. Kraft, H. Eschrig, A.N. Yaresko, A.Ya. Perlov, J. Phys.: Condens. Matter 8 (1996) 5769.
[10] J. van Ek, M. Mclaren, Phys. Rev. B 56 (1997) R2924.
[11] T. Kusakabe, K. Kyuno, S. Asano, J. Magn. Magn. Mater. 126 (1993) 535.
[12] G.Y. Guo, H. Ebert, Phys. Rev. B 51 (1995) 12633.
[13] J.-G. Ha, K. Kyuno, R. Yamamoto, J. Phys.: Condens. Matter 8 (1996) 677.
[14] S. Uba, L. Uba, A.N. Yaresko, Ya.A. Perlov, V.N. Antonov, R. Gontarz, Phys. Rev. B 53 (1996) 6526.
[15] T. Kraft, P.M. Oppeneer, V.N. Antonov, H. Eschrig, Phys. Rev. B 52 (1995) 3561.
[16] P.M. Oppeneer, M.S.S. Brooks, V.N. Antonov, T. Kraft, H. Eschrig, Phys. Rev. B 53 (1996) R10437.
[17] A.N. Yaresko, P.M. Oppeneer, Ya.A. Perlov, V.N. Antonov, T. Kraft, H. Eschrig, Phys. Rev. B 77 (1996) 5253.
[18] C.S. Wang, J. Callaway, Phys. Rev. B 9 (1974) 4897.
[19] M. Singh, C.S. Wang, J. Callaway, Phys. Rev. B 11 (1975) 287.
[20] T. Katayama, N. Nakajima, N. Okusawa, Y. Miyauchi, T. Koide, T. Shidara, Y. Suzuki, S. Yuasa, J. Magn. Magn. Mater. 177–181 (1998) 1251.
[21] O.K. Andersen, Phys. Rev. B 12 (1975) 3060.
[22] D.D. Koelling, G. Arbman, J. Phys. F 5 (1975) 2041.
[23] M. Weinert, J. Math. Phys. 22 (1981) 2433.
[24] J.M. Soler, A.R. Williams, Phys. Rev. B 40 (1989) 1560.
[25] J.M. Soler, A.R. Williams, Phys. Rev. B 42 (1990) 9728.
[26] J.M. Soler, A.R. Williams, Phys. Rev. B 47 (1993) 6784.
[27] D.D. Koelling, B.N. Harmon, J. Phys. C 10 (1977) 3107.
[28] P.E. Blöchl, O. Jepsen, O.K. Andersen, Phys. Rev. B 49 (1994) 16223.
[29] K.B. Hathaway, H.J.F. Jansen, A.J. Freeman, Phys. Rev. B 31 (1985) 7603.
[30] H. Miyazawa, T. Oguchi, unpublished.
[31] D. Weller, G.R. Harp, R.F.C. Farrow, A. Cebollada, J. Sticht, Phys. Rev. Lett. 72 (1994) 2097.
[32] H. Oka, H. Miyazawa, T. Oguchi, unpublished.
[33] O. Jepsen, D. Glötzel, A.R. Mackintosh, Phys. Rev. B 23 (1981) 2684.
[34] H. Mårtensson, P.O. Nilsson, Phys. Rev. B 30 (1984) 3047.
[35] L. Hedin, Phys. Rev. 139 (1965) A796.
[36] M.S. Hybertsen, S.G. Louie, Phys. Rev. B 34 (1986) 5390.
[37] F. Aryasetiawan, Phys. Rev. B 46 (1992) 13051.
[38] G.S. Krinchik, V.A. Artemev, Sov. Phys. JETP 26 (1968) 1080.